Available online at www.sciencedirect.com
SCIENCE DIRECT
Journal of Power Sources 158 (2006) 52–59
JOURNAL OF POWER SOURCES
www.elsevier.com/locate/jpowsour

Cycle analysis of planar SOFC power generation with serial connection of low and high temperature SOFCs

Takuto Araki [a,*], Takahiro Ohba [a], Shinya Takezawa [a], Kazuo Onda [a], Yoshinori Sakaki [b]

[a] *Department of Electrical and Electronic Engineering, Toyohashi University of Technology, 1-1 Hibarigaoka, Tenpaku, Toyohashi, Aichi 441-8580, Japan*
[b] *Electric Power Research and Development Center, Chubu Electric Power Co., Japan*

Received 5 July 2005; received in revised form 31 August 2005; accepted 2 September 2005
Available online 19 October 2005

Abstract

Solid oxide fuel cells (SOFCs) can be composed of solid components for stable operation, and high power generation efficiency is obtained by using high temperature exhaust heat for fuel reforming and bottoming power generation by a gas turbine. Recently, low-temperature SOFCs, which run in the temperature range of around 600 °C or above and give high power generation efficiency, have been developed. On the other hand, a power generation system with multi-staged fuel cells has been proposed by the United States DOE to obtain high efficiency. In our present study, a power generation system consisting of two-staged SOFCs with serial connection of low and high temperature SOFCs was investigated. Overpotential data for the low-temperature SOFC used in this study are based on recently published data, while data for high-temperature SOFC are based on our previous study. The numerical results show that the power generation efficiency of the two-staged SOFCs is 50.3% and the total efficiency of power generation with gas turbine is 56.1% under standard operating conditions. These efficiencies are a little higher than those by high-temperature SOFC only.

Keywords: Two-staged serial SOFCs; Low temperature SOFC; Lanthanum gallate; High temperature SOFC; Cycle analysis

1. Introduction

Solid oxide fuel cells (SOFCs) are made entirely of solid materials for high reliability. The high temperature exhaust heat obtained simultaneously with power generation is used in fuel reforming, bottoming power generation, and the regenerative heating of fuel and air, as a result of which the total power generation efficiency of the entire cycle is high. In addition to the conventional high temperature SOFC that uses Y_2O_3 stabilized ZrO_2 as the electrolyte, a recent low temperature SOFC with a lanthanum gallate electrolyte that can be operated from about 600 °C has shown superior power generation characteristics [1], thereby expanding the operating temperature range of SOFCs. Since the power generation efficiency of a fuel cell is higher than that of a gas turbine, which is used as a bottoming power generator in the integrated SOFC-gas turbine cycle, expansion of the operating temperature range of SOFC is promising for increased system power generation efficiency. The United States Department of Energy (DOE), on the other hand, has investigated ways to achieve high power generation efficiency of 80% and has proposed a multi-staged fuel cell system with five serial stages of fuel cells in order to reduce the regenerative heat for fuel and air, and to extend the operating temperature range of fuel cells [2]. We have conducted previously cycle analyses of the combined cycle of high temperature SOFC and gas turbine, with consideration of realistic losses from overpotentials and other factors [3–4]. In the present study we propose a planar SOFC with two stages of low and high temperature SOFCs placed in series. We also speculate how much the combined cycle efficiency of two-staged SOFCs and gas turbine can actually be improved in the several hundred kW class of power generation, with investigation of the available data on overpotentials and other physical properties of low temperature SOFC [5–8].

1.1. Low and high temperature SOFCs of planar type

1.1.1. Cell configuration

Fig. 1 shows the configuration of a planar unit cell investigated in this study. The unit cell for both low and high

* Corresponding author. Tel.: +81 532 44 6728; fax: +81 532 44 6728.
E-mail address: araki@eee.tut.ac.jp (T. Araki).

0378-7753/$ – see front matter © 2005 Elsevier B.V. All rights reserved.
doi:10.1016/j.jpowsour.2005.09.003

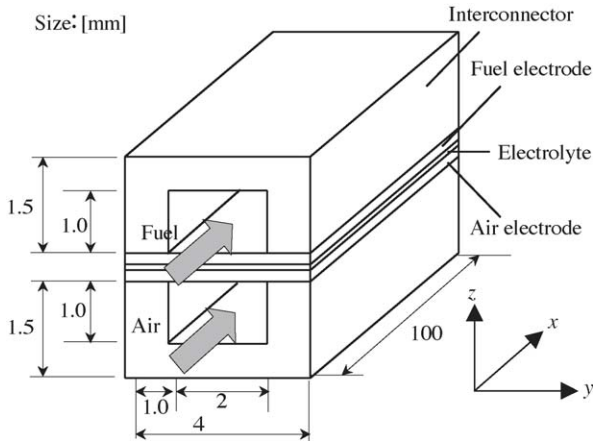

Fig. 1. Configuration of a unit cell.

temperature SOFCs is assumed to be a planar and parallel-flow type with similar sizes, as shown in Fig. 1. The materials and thickness of the electrodes and electrolyte for both low and high temperature systems are shown in Table 1. The interconnector for the low temperature system is SUS (stainless steel), and that for the high temperature system is $La_{1-x}Sr_xCrO_3$. The physical properties used for the low temperature SOFC were obtained by referring to SOFC studies [5–8] using lanthanum gallate electrolytes, and those for high temperature SOFC by referring to our previous reports [3,4]. Tables 2 and 3 show the thermal conductivity and resistivity for each element of low and high temperature SOFCs, respectively. The resistivity at temperature T_e of low and high temperature electrolytes, ρ_{e_low} (Ω m) [8] and ρ_{e_high} (Ω m) [9], is described by Eqs. (1) and (2), and the physical properties that have not been published for a low temperature system were assumed to be the same as for high temperature system.

$$\rho_{e\_low} = 0.03997 + 0.58731 \exp\left(\frac{T_e - 823.15}{86.47858}\right) \quad (1)$$

$$\rho_{e\_high} = 3.61 \times 10^{-5} \exp\left(\frac{10092}{T_e}\right) \quad (2)$$

1.1.2. Cell performance analysis

Two-dimensional conservation equations for charge, mass, and energy in both the low and high temperature systems are discretized together with an equivalent electric circuit of the fuel cell along the direction of gas flow and membrane thickness. The distribution of species concentration, current density, potential, and so on within the cell was analyzed numerically using the control volume method [3,4]. We first set operating conditions for the calculations, such as cell size, mean current density, and overall fuel and air utilization rates for both the low and high temperature systems. Then the inlet gas composition was decided for the low temperature SOFC. Next, with some mean electrolyte temperature of the low temperature cell as a parameter, calculations were started from the low temperature SOFC, and the current and temperature distributions were made to converge. The gas composition and temperature obtained at the low temperature SOFC outlet were then taken as the high temperature inlet condition, and calculations for the high temperature SOFC were carried out the same as for the low temperature SOFC. Therefore the mean temperature of high temperature SOFC was calculated from the mean temperature of low temperature SOFC and the operation conditions. Here, the activation overpotential V_{act_low} of the low temperature SOFC is given by Eq. (3), assuming a constant overpotential resistance from published data [5–8], and V_{act_high} of the high temperature SOFC by Eq. (4) from our previous reports [3–4]. Similar to V_{act_high}, V_{act_low} should be given by a temperature dependent function, but the temperature dependent V_{act_low} has not been published elsewhere.

$$V_{act\_low} = \frac{2.5 \times 10^{-5}}{w\,dx} I_e \quad (3)$$

$$i_e = i_0 \left\{ \exp\left(\frac{2FV_{act\_high}}{RT}\right) - \exp\left(\frac{-(2 \text{ or } 1)FV_{act\_high}}{RT}\right) \right\} \quad (4)$$

Here, w is cell width, dx is segmented length along flow direction, F is the Faraday constant, R is the gas constant, T_e is electrolyte temperature, I_e is current through electrolyte, i_e is current density through electrolyte, and i_0 is the exchange current density as a function of oxygen partial pressure. In our previous study [3], fuel was reformed internally in the cell to suppress the temperature rise of high temperature SOFC, but in the present study methane fuel was reformed completely at an external reformer and the reformed gas was introduced to the low temperature SOFC, since the cycle configuration would become too complex

Table 1
Compositions of electrolyte and electrode for low and high temperature SOFC

SOFC Type	Electrolyte (thickness: mm)	Fuel electrode (thickness: mm)	Air electrode (thickness: mm)	Interconnector
Low temperature	$La_{0.8}Sr_{0.2}Ga_{0.8}Mg_{0.15}Co_{0.05}O_{3-\delta}$ (200×10^{-3})	$Ni/Ce_{0.8}Sm_{0.2}O_2$ (1)	$Sm_{0.5}Sr_{0.5}CoO_3$ (1)	SUS
High temperature	YSZ (100×10^{-3})	Ni-YSZ (70×10^{-3})	$LaSrMnO_3$ (70×10^{-3})	$La_{1-x}Sr_xCrO_3$

Table 2
Physical properties of low temperature SOFC

Element	Electrolyte	Fuel electrode	Air electrode	Fuel side interconnector	Air side interconnector
Thermal conductivity (W m^{-1} K^{-1})	2.7	11	2.2	16.3	16.3
Resistivity (Ω m)	Eq. (1)	1.0×10^{-5}	1.3×10^{-4}	7.4×10^{-7}	7.4×10^{-7}

Table 3
Physical properties of high temperature SOFC

Element	Electrolyte	Fuel electrode	Air electrode	Fuel side interconnector	Air side interconnector
Thermal conductivity ($W\,m^{-1}\,K^{-1}$)	2.7	11	2.2	2.34	2.34
Resistivity ($\Omega\,m$)	Eq. (2)	1.0×10^{-5}	1.3×10^{-4}	3.2×10^{-3}	1.6×10^{-3}

with internal reforming. Further, our cycle analyses assumed the shift reaction to be in thermal equilibrium, since the reaction rate is considered to be fast.

1.2. Standard conditions and representative potential, current density, and temperature distributions

Standard cycle operating conditions were mean temperature of 750 °C for the low temperature SOFC (defined as mean temperature [3] of the cell electrolyte), mean current density of 0.3 A cm^{-2}, cell pressure of 1.0 MPa, total fuel utilization rate of 85% (42.5% in the low temperature SOFC, 42.5% in the high temperature SOFC based on methane), total air utilization rate of 30% (15% in the low temperature SOFC, 15% in the high temperature SOFC), fuel recirculation rate of 30%, and air recirculation rate 10%. First, the power generation performances of low and high temperature SOFCs were calculated in detail, and then the overall performance of the combined cycle was calculated the same as in previous studies [3,4]. Each one of these parameters was then changed to see its effect on total cycle performance.

The potential distribution and temperature and current density distributions for the low temperature SOFC under these standard conditions are shown in Figs. 2 and 3, respectively. The potential distribution and temperature and current density distributions for the high temperature SOFC are shown in Figs. 4 and 5. As seen in the figures, since the overpotential was lower in the low temperature SOFC than in the high temperature SOFC, the cell voltage and power generation performance of the former were superior to those of the latter. Moreover, since temperature changes in overpotential other than electrolyte resistance overpotential were not introduced, the current density distribution was similar to the distribution of the Nernst poten-

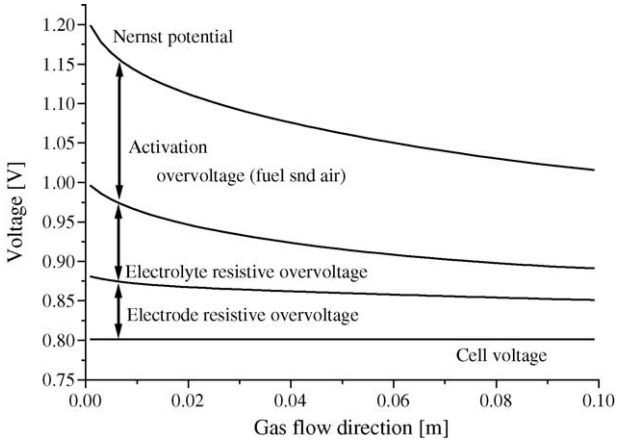

Fig. 2. Voltage distribution of low temperature SOFC.

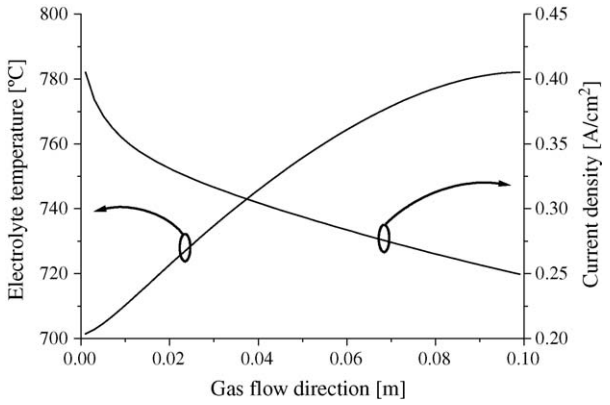

Fig. 3. Temperature and current density distributions of low temperature SOFC.

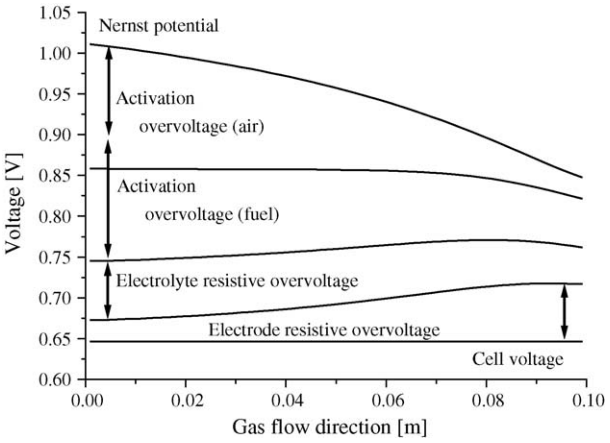

Fig. 4. Voltage distribution of high temperature SOFC.

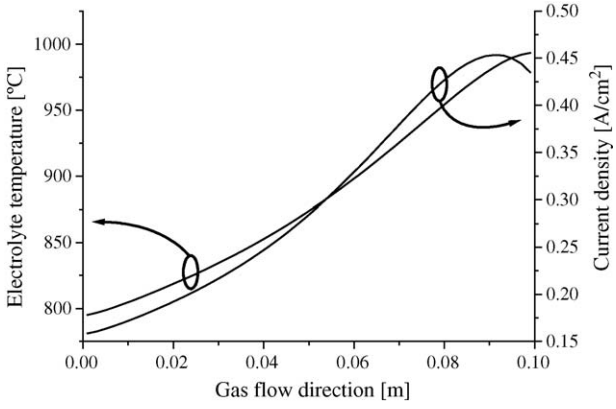

Fig. 5. Temperature and current density distributions of high temperature SOFC.

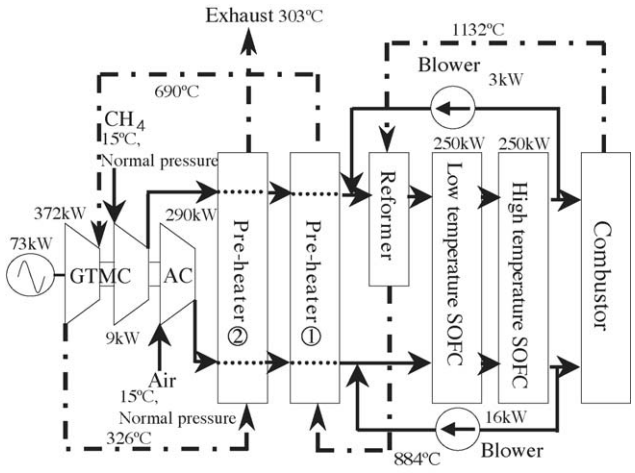

Fig. 6. Two-staged low and high temperature SOFC system.

tial, and the temperature distribution was small owing to the use of SUS with high thermal conductivity in the interconnector. At the high temperature SOFC the heat generation by overpotential in the latter half of the cell was great, and the temperature rise was large, thus, activation overpotential and electrolyte resistance became small, as a result of which current density in the latter half of the cell was large, and the temperature distribution was also larger than in the low temperature SOFC.

1.3. Configuration of SOFC-gas turbine combined power generation system

1.3.1. Configuration of cycle

Fig. 6 shows a cycle diagram of the combined power generation system with a two-staged SOFC of low and high temperature SOFCs arranged in series as a topping cycle, and a gas turbine as a bottoming cycle. The fuel of methane is 100% reformed in the external reformer, and supplied to the low temperature SOFC. The gas that comes from the low temperature SOFC is then supplied directly to the high temperature SOFC. Other structures are basically the same as previously reported [3]. A part of the depleted fuel and air emitted from the high temperature SOFC is recirculated by a blower to make the cell temperature distribution more uniform to alleviate thermal stress, and to self-supply water vapor for reforming. The exhaust fuel and air that is not recirculated is burned in a combustor, and then the combustion gas flows into an external reformer for heating. Next, the gas flows into a pre-heater 1 to regeneratively heat fresh fuel and air for SOFC, and generate power in a gas turbine (GT) driving an air compressor (AC) and a methane compressor (MC). Afterward, the combustion gas flows into a pre-heater 2 to regeneratively heat the compressed fuel and air.

1.3.2. Calculation conditions of cycle

As in a previous study, the heat balance of individual component in the cycle analysis is obtained by the entropy balance at inlet and outlet of each component, and turbine output and compressor input are estimated by using appropriate adiabatic efficiencies [3]. After setting the operating conditions, the cycle calculation starts from the low and high temperature SOFC calculations and the calculations converge. Then the cycle calculation proceeds to the energy balance of the total system. Table 4 summarizes the basic equations, various efficiencies, and other conditions used in the cycle calculations. Here, M is the molar flow rate, C_p is the molar specific heat at constant pressure, $\Delta H(T_0)$ is the entropy difference at standard temperature, T_{in} is input temperature, the suffixes i, j are for gas species i, j, Q is amount of exchange heat, ϕ is pressure ratio, κ is specific heat ratio, η_{GI} is adiabatic efficiency for gas turbine, and $\eta_{\text{Comp,Blow}}$ is adiabatic efficiency for compressor or blower.

1.4. Numerical results

Centered on standard conditions, single parameters only were changed as follows to identify the effect produced by each parameter on cycle performance. In the following analyses, the solid circles (●) indicate the generation efficiency of the high temperature SOFC only (net output from high temperature SOFC/thermal input to cycle based on HHV), the solid squares (■) indicate the generation efficiency of low temperature SOFC only, the solid triangles (▲) indicate the generation efficiency

Table 4
Calculation equations and various efficiencies for cycle analyses

Enthalpy income and expenditure	$\sum_i M_i \left(\int_{T_0}^{T_{\text{in}}} C_{p_i}\, \mathrm{d}T + \Delta H_i(T_0) \right) \pm Q = \sum_j M_j \left(\int_{T_0}^{T_{\text{out}}} C_{p_j}\, \mathrm{d}T + \Delta H_j(T_0) \right)$
Gas-turbine output	$W_{\text{Gas turbine}} = \sum_i \{ M_i C_{p_i} T_{\text{in}} (1 - \phi^{-\kappa-1/\kappa}) \eta_{\text{GT}} \}$
Compressor and blower power	$W_{\text{Compressor,Blower}} = \sum_i \{ M_i C_{p_i} T_{\text{in}} (\phi^{\kappa-1/\kappa} - 1) / \eta_{\text{Comp,Blow}} \}$
Heat loss to heat input at SOFC	1%
Heating ratio of air and fuel at pre-heater 1	90%
Heating ratio of air and fuel at pre-heater 2	10%
Adiabatic efficiency of gas turbine	87%
Adiabatic efficiency of compressor and blower	77%
Inverter efficiency	95%
External reforming ratio	100%
Pressure ratio of high temperature blower	1.05
Heat loss to exchanging heat at PH 1 and 2	3%

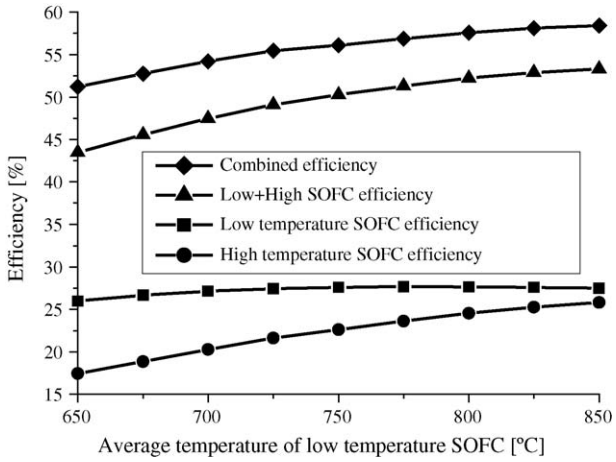

Fig. 7. Change in power generation efficiency with mean cell temperature in low temperature SOFC.

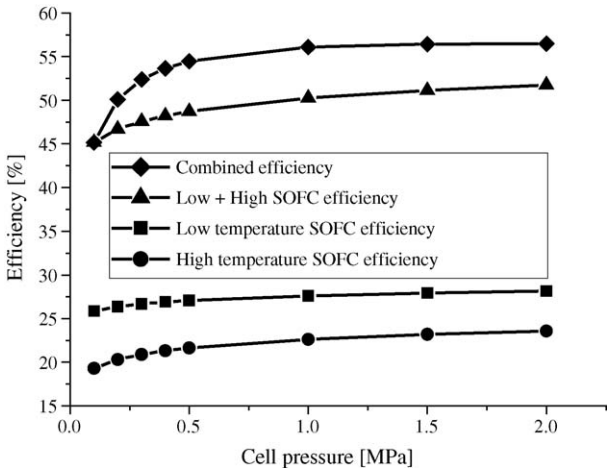

Fig. 8. Change in power generation efficiency with cell pressure.

added by both low and high temperature SOFCs, and the solid rhombuses (♦) indicate the combined generation efficiency of SOFC and GT. The main results of cycle analyses under the standard condition are shown in Fig. 6.

1.4.1. Efficiency changes with mean temperature of low temperature SOFC

Fig. 7 shows the changes in various power generation efficiencies with changes in mean temperature of the low temperature SOFC. Since the overpotential is lower in the low temperature SOFC than in the high temperature SOFC, the efficiency of low temperature SOFC is higher than that of high temperature SOFC. Since increasing the mean temperature of the low temperature SOFC reduces the electrolyte resistance in both the low and high temperature SOFCs, all generation efficiencies increase. The mean temperature of high the temperature SOFC increases as the mean temperature of the low temperature SOFC increases. As a result, the activation overpotential of the high temperature SOFC decreases, with a greater increase in generation efficiency in the high temperature SOFC than in the low temperature SOFC. The Nernst potential decreases with increase of temperature, and the overpotential of the low temperature SOFC does not decrease so much with temperature. Therefore the generation efficiency of the low temperature SOFC becomes saturated with increase of temperature. The allowable upper-limit temperature of the low temperature SOFC may decide the maximum efficiency of both the low and high temperature SOFCs. In the bottoming gas turbine cycle, increase in the mean temperature of the low temperature SOFC causes an increase in the inlet temperature of the low temperature SOFC. This means that amount of inlet gas preheat increases, and the turbine inlet temperature declines with decreasing turbine output. However, since the increase in power generation efficiency of SOFCs is larger than the decrease in power generation efficiency of GT, the combined efficiency increases.

1.4.2. Efficiency changes with cell pressure

Fig. 8 shows the changes in power generation efficiencies with cell pressure. Raising the cell pressure causes an increase in the Nernst potential. When the oxygen partial pressure increases in the high temperature SOFC, the activation overpotential at air electrode declines [3,4], resulting in an increase in power generation efficiency. However, the efficiency improvement with cell pressure is soon saturated at near 1 MPa. In the bottoming gas turbine cycle, increasing the operating pressure leads to some decrease in the cell outlet temperature. However, an increase in compressor outlet temperature causes an increase in the turbine inlet temperature due to the decreased input for air preheating, resulting in an increase of gas turbine output. When the pressure increases too much, however, the turbine net output declines and the combined efficiency becomes saturated, since the compressor power increases with the pressure increase.

1.4.3. Efficiency changes with mean current density

Fig. 9 shows the changes in power generation efficiencies with mean current density. Increasing the current density increases the SOFC overpotential loss, resulting in a linear decrease of generation efficiencies. However, since the temperature elevation with increasing current density is large at high temperature SOFC, the activation overpotential and electrolyte resistance decrease greatly. Therefore the decreasing rate of the

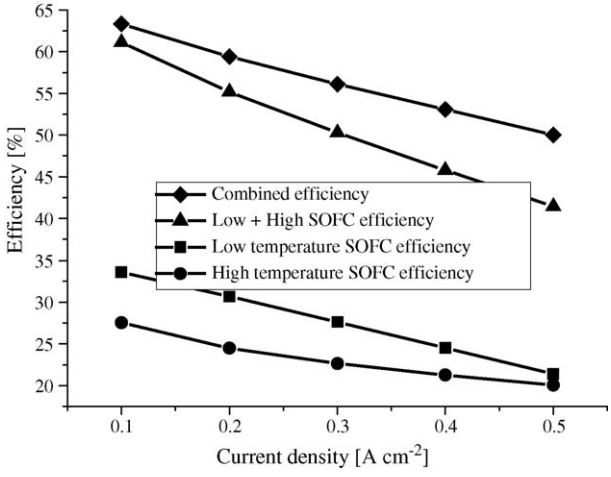

Fig. 9. Change in power generation efficiency with current density.

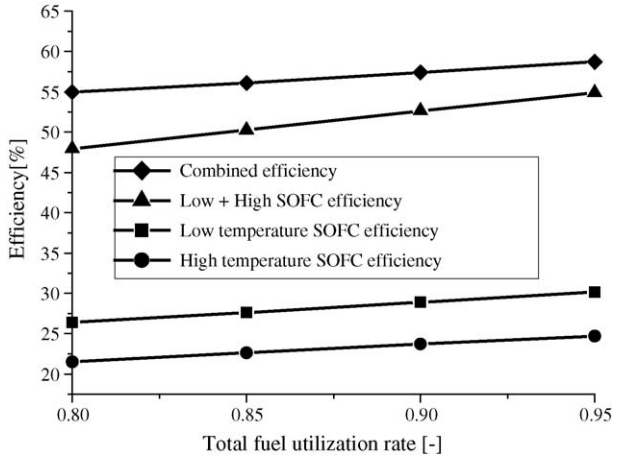

Fig. 10. Change in power generation efficiency with total fuel utilization rate.

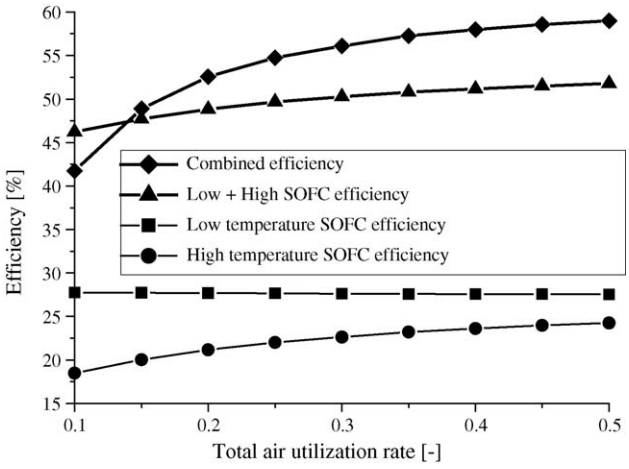

Fig. 11. Change in power generation efficiency with total air utilization rate.

high temperature SOFC output is smaller than that of the low temperature SOFC. In the bottoming gas turbine cycle, since SOFC outlet temperature increases with increase of the current density, the turbine inlet temperature increases together with the increasing turbine output. However, since the decrease in SOFC power generation efficiency is larger than the increase in gas turbine efficiency, the combined efficiency of the total cycle declines.

1.4.4. Efficiency changes with total fuel utilization rate

Fig. 10 shows the changes in power generation efficiencies with total fuel utilization rate (equal share in low and high temperature SOFCs). Increases in the fuel utilization rate bring decreased cell voltage, but the efficiency improvement from higher fuel utilization rate is significant, resulting in increasing power generation efficiencies. In the bottoming gas turbine cycle, when the energy converted at SOFC increases with increase in fuel utilization rate, the thermal input to gas turbine decreases. Therefore, the turbine inlet temperature drops with decreasing turbine output. However, the efficiency improvement by SOFCs is larger, so the combined efficiency increases.

1.4.5. Efficiency changes with total air utilization rate

Fig. 11 shows the changes in power generation efficiencies with total air utilization rate (equal share in low and high temperature SOFCs). Raising the air utilization rate results in slightly lower cell voltage with decreasing power generation efficiency at the low temperature SOFC. However, when air supply to the high temperature SOFC becomes smaller, the mean temperature increases with the decreasing electrolyte resistance and activation overpotential, which lead to increasing cell voltage and power generation efficiency. In the bottoming gas turbine cycle, when the air utilization rate increases the supplied air decreases together with the reduced amount of preheat. Therefore, the gas turbine inlet temperature increases, and turbine output becomes higher. At a total air utilization rate of 0.1, however, the air compression input becomes larger than the turbine net output, and then the combined efficiency becomes lower than the power generation efficiency by low and high temperature SOFCs. When the total air utilization rate is 0.5, on the other hand, the temperature rise at high temperature SOFC is 298 °C and the outlet temperature becomes as high as 1094 °C; thus, the allowable temperature of high temperature SOFC may limit the power generation efficiency.

1.4.6. Efficiency changes with fuel recirculation rate

Fig. 12 shows the changes in power generation efficiencies with fuel recirculation rate. The variable range for the fuel recirculation rate is limited by the water flow rate needed for reforming and constraints due to the system configuration. Increasing the fuel recirculation rate brings the decreased fuel concentration, resulting in a slight decline in power generation efficiencies of the low and high temperature SOFCs. In the bottoming gas turbine cycle, when the fuel recirculation rate increases, the temperature of raw fuel supplied to the reformer drops, and the amount of fuel preheat decreases, resulting in the increase of turbine inlet temperature with slightly increasing turbine output. However, the combined efficiency declines because of the fairly large drop in SOFC power generation efficiency. Since the lower limit of the steam/carbon ratio without any carbon deposition depends on the performance of reformer, further investigations are necessary to match the recirculation rate to reformer performance.

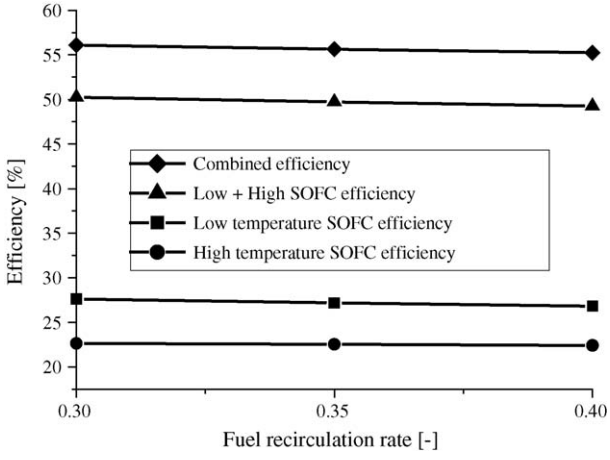

Fig. 12. Change in power generation efficiency with fuel recirculation rate.

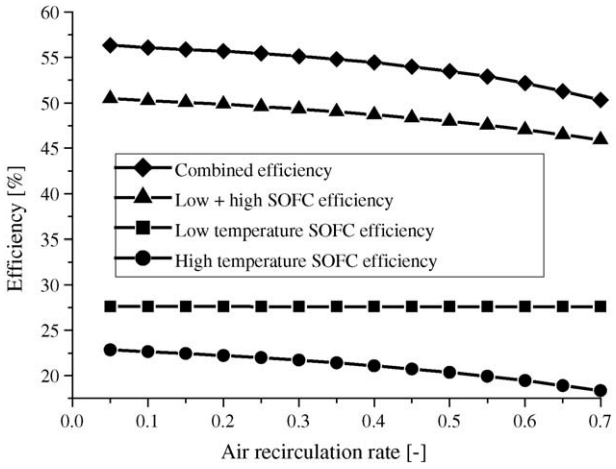

Fig. 13. Change in power generation efficiency with air recirculation rate.

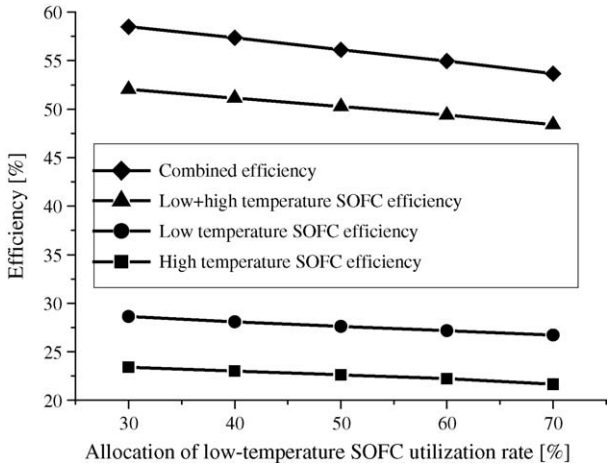

Fig. 14. Change in power generation efficiency by allocation of low-temperature SOFC utilization rate.

1.4.7. Efficiency changes with air recirculation rate

Fig. 13 shows the changes in power generation efficiencies with air recirculation rate. With increases in the air recirculation rate the temperature distribution in the low temperature SOFC, which has a fixed mean cell temperature, becomes uniform and the efficiency of low temperature SOFC increases slightly. However, the mean cell temperature of high temperature SOFC decreases and the overpotential becomes greater, resulting in lower power generation efficiency. In the bottoming gas turbine cycle, increasing the air recirculation rate causes the SOFC outlet temperature to decline, as a result of which both the turbine inlet temperature and output power decrease.

1.4.8. Efficiency changes with allocation of utilization rate

In the above analyses, we divided the utilization rate half and half between the low and high temperature SOFCs. Here the allocation of both fuel and air utilization rates for the low and high temperature SOFCs is changed, as shown in Table 5, to calculate efficiency changes. The total fuel utilization rate is fixed at 85%, and the total air utilization rate is fixed at 30%.

Fig. 14 shows the changes in power generation efficiencies with allocation of the utilization rate. As the allocation of utilization rate becomes large at low temperature SOFC, the generation efficiencies of both low and high temperature SOFCs decrease. When the allocation of utilization rate becomes larger at the low temperature SOFC, the low temperature cell lengthens under the calculation condition of assumed mean current density, and the cell voltage of the low temperature SOFC decreases. Since the activation overpotential of low temperature SOFC was assumed to be independent of temperature, the cell voltage distribution decreases along the gas flow as shown in Fig. 2, together with the Nernst potential. Therefore the cell voltage drops as the cell becomes longer. In addition, as the allocation of utilization rate at the low temperature SOFC becomes larger, the amount of heat release at the low temperature SOFC is smaller than that at the high temperature SOFC, since the low temperature SOFC has a higher efficiency. Therefore the mean temperature of the high temperature SOFC decreases with increasing allocation at the low temperature SOFC, resulting in the larger activation and resistance overpotentials and lower cell voltage of high temperature SOFC.

When the mean temperature of the low temperature SOFC becomes a little over 750 °C, there is a temperature range where the high temperature SOFC can work with a little higher efficiency, as expected from Fig. 7. In the future, therefore, after clarifying the upper temperature limits of low and high temperature SOFCs, there is a need to determine the optimum operating conditions for two-staged serial SOFCs.

Table 5
Allocation of utilization rate

SOFC type	Allocation of utilization ratio (%)				
Low temperature SOFC	30	40	50	60	70
High temperature SOFC	70	60	50	40	30

1.4.9. Comparison with high temperature SOFC single cycle

Finally, the two-staged SOFC cycle in the present study is compared with our single cycle with high temperature SOFC only [3]. The operating conditions for the high temperature, single-staged SOFC cycle used in this comparison are mean cell temperature of 900 °C, fuel utilization rate of 85%, air utilization rate of 30%, current density of 0.3 A cm^{-2}, cell pressure of 1.0 MPa, fuel and air recirculation rates of 50%, and external reforming rate of 50% [3]. This single cycle of high temperature SOFC shows an SOFC power generation efficiency of 45.1%, and a combined cycle efficiency of 54.7%. In contrast, the two-staged SOFC cycle in the present study (mean temperature of low temperature SOFC 750 °C, mean temperature of high temperature SOFC 884 °C) shows an SOFC power generation efficiency of 50.3% and a combined cycle efficiency of 56.1% at standard operating conditions. The two-staged SOFC cycle in this study has both higher SOFC power generation efficiency and combined cycle efficiency. This is because the power generation efficiency of low temperature SOFC is about 5% higher than that of high temperature SOFC. Also, the thermal input to gas turbine in the two-staged SOFC cycle is higher due to the decreased

amount of fuel and air preheat. The reason the combined cycle efficiency of the two-staged SOFC increases to only 5% higher than the single SOFC cycle is that much heat is required for 100% external reforming in the two-staged SOFC cycle.

2. Conclusion

Based on currently available data, a program to analyze the power generation performance of low temperature planar SOFC was created. A combined power generation cycle having low and high temperature SOFCs arranged in series and a gas turbine was analyzed. The SOFC power generation efficiency was found to be 50.3% and the combined cycle power generation efficiency to be 56.1% under standard operation conditions of mean cell temperature for low temperature SOFC of 750 °C, mean current density of 0.3 A cm^{-2}, cell pressure of 1.0 MPa, total fuel utilization rate of 85%, total air utilization rate of 30%, fuel recirculation rate of 30%, air recirculation rate of 10%, and external reforming rate of 100%. Further, by changing the operating parameters, mean temperature of low temperature SOFC, cell pressure, mean current density, total fuel utilization rate, total air utilization rate, fuel recirculation rate, air recirculation rate, and allocation of both fuel and air utilization rates for low and high temperature SOFCs, we studied their effects on power generation efficiencies of low and high temperature SOFCs, and combined cycle. We compared the two-staged SOFC cycle with a single cycle of high temperature SOFC only, which had an SOFC power generation efficiency of 45.1% and a combined power generation efficiency of 54.7%. This was done under operation conditions of mean cell temperature of 900 °C, fuel and air recirculation rates of 50%, external reforming rate of 50%, and other operation conditions the same as with the two-staged SOFC cycle. The results revealed that the two-staged SOFC cycle has both higher SOFC power generation efficiency and combined cycle efficiency.

References

[1] T. Ishihara, H. Matsuda, Y. Takita, J. Am. Chem. Soc. 116 (1994) 3801.
[2] T.J. George, K.D. Lyons, R. James, Fuel Cell Semin. (1998).
[3] K. Onda, T. Iwanari, N. Miyauchi, A. Ito, K. Ito, T. Ohba, Y. Sakaki, S. Nagata, J. Electrochem. Soc. 150 (2003) A1569.
[4] M. Iwata, T. Hikosaka, M. Morita, T. Iwanari, K. Ito, K. Onda, Y. Esaki, Y. Sakaki, S. Nagata, Solid State Ionics 132 (2000) 297.
[5] A. Monma, T. Kato, K. Nozaki, A. Negishi, K. Kato, Y. Kaga, A. Nagata, K. Takano, T. Inagaki, H. Yoshida, K. Hosoi, K. Hoshino, T. Akbay, J. Akikusa, Proceedings of the 11th Symposium on Solid Oxide Fuel Cells in Japan, 2002, p. 13 (in Japanese).
[6] T. Kato, K. Nozaki, A. Negishi, K. Kato, A. Monma, Y. Kaga, S. Nagata, K. Takano, T. Inagaki, H. Yoshida, K. Hosoi, K. Hoshino, T. Akbay, J. Akikusa, J. Power Sources 133 (2004) 169.
[7] A. Momma, T. Kato, K. Nozaki, A. Negishi, K. Kato, Y. Kaga, S. Nagata, K. Takano, T. Inagaki, H. Yoshida, K. Hosoi, K. Hoshino, T. Akbay, J. Akikusa, Proceedings of the Electrochemical Society 2003–2007, 2003, p. 1186.
[8] K. Kuroda, I. Hashimoto, K. Adachi, J. Akikusa, Y. Tamou, N. Komada, T. Ishihara, Y. Takita, Solid State Ionics 132 (2000) 199.
[9] S. Nagata, A. Momma, T. Kato, Y. Kasuga, J. Power Sources 101 (2001) 60.